RSC Advances

ROYAL SOCIETY OF CHEMISTRY

www.rsc.org/advances

Fabrication of translucent nanoceramics via a simple filtration method

Yixiao Cai[1], Song Chen[1], Kathryn Grandfield[2], Håkan Engqvist[1], Wei Xia[1*]

[1]Applied Materials Science, Department of Engineering Sciences, Ångström Laboratory, Uppsala University, Uppsala, Sweden

[2] Department of Materials Sciences and Engineering, McMaster University, Hamilton, Ontario, Canada

Abstract

Generally, particle packing density, and grain size and morphology are the important factors that affect the transparency of ceramics. In order to achieve better transparency of ceramics, efforts should be developed to eliminate or minimize light scattering or absorption. Therefore the porosity and the size of crystals in a ceramic body should be strictly controlled. Typical transparent ceramics are fabricated by pressure-assisted sintering techniques such as hot isostatic pressing (HIP), spark plasma sintering (SPS), and pressure-less sintering (PLS). However, a simple energy efficient production method remains a challenge. In this study, we describe a simple fabrication process via a facile filtration system that can fabricate translucent hydroxyapatite based ceramics. The translucent pieces yielded from filtration exhibit optical transmittance that was confirmed by UV spectroscopy. Briefly, the morphology and size of ceramic nanoparticles, the filtration pressure and filtration time are important parameters discussed. Compared with different hydroxyapatite nanoparticles, spherical nanoparticles are easy to form a densely packed structure, followed by sintered ceramics. When strontium contents in HA increase, the morphology of HA changed from nano-spheres to nano-rods, following a decrease in transparency. A pressure filtration model combining Darcy's law and Kozeny-Carman relation has been discussed to simulate and explain why the translucent ceramics can be fabricated via such a simple process. This method could be further applied to prepare other translucent functional ceramics by controlling the size and morphology of ceramic particles.

Keywords: Translucent ceramics, Hydroxyapatite, Bioceramic, Filtration

1 Introduction

Transparent polycrystalline ceramics exhibit improved heat resistant and strength compared to single crystals, even though they have lower visible transmittance[1,2]. There is growing interest in applying such ceramic-based materials in biomedicine and biomaterials, particularly in the application of direct observation of bone matrix in vitro on bioceramics and percutaneous devices[3,4]. A transparent ceramic should have a compact and pore-less microstructure since pores often contribute to opacity in a ceramic[2, 5, 6]. However, it is a challenge to achieve full densification of polycrystalline ceramics since both a good vacuum level, as well as high temperature and pressure are required during fabrication[7]. Efforts should be considered and made to minimize light scattering to achieve transparency in a ceramic.

Hydroxyapatite (HA), considered as a polycrystalline ceramic biomaterial having bioactive and biocompatible properties, has been widely used in interdisciplinary fields of science including physics, chemistry, biology, and medicine[8–11]. HA exhibits osteoconductive, non-toxic and non-immunogenic properties especially in the repair of bones and teeth[12,13]. However, it is difficult to directly observe HA-cell or HA-tissue interactions with conventional light microscopy methods because HA is normally opaque. Making an HA ceramic transparent will therefore extend its biomedical applications. For example, Takikawa et al[14] observed bone matrix formation on transparent HA ceramics simply and dynamically using light microscopy, and John et al[15] investigated bone remodeling on transparent HA ceramic. Furthermore, a transparent HA ceramic can be a good candidate for percutaneous devices since it can work as a window for observation of changes inside. Also, several research groups are continuously investigating the growth of osteoblast or osteoblast-like cells on transparent hydroxyapatite ceramics[16,17]. Aoki et al.[18] used HA device for long-term blood pressure and deep body temperature detection. In fact, for better detection by modern bio-imaging optical techniques, the transparent HA ceramics can play significant roles here for its excellent biocompatibility. Fujimori et al[16]. detected osteogenic differentiation cascade of living stem cells on transparent HA ceramics. Thus, transparent HA ceramics can function as windows to track instant biological changes. Generally, to achieve transparent HA ceramics, densification is essential to reduce the porosity. Recently, spark plasma sintering (SPS)[7,19,20], hot isostatic pressing (HIP)[21–23], and pressure-less sintering (PLS)[24] are examples of hydrothermal methods that have been recently used. For instance, Roy et al.[25] fabricated transparent hydroxyapatite ceramics at ambient-pressure pressure by microwave processing as well as by conventional sintering. Watanabe et al.[26] fabricated transparent HA by pulse electric current sintering method.

In this paper, to best of the author's knowledge, we describe the first fabrication of translucent HA and strontium substituted HA (SrHA) ceramics by a simple filtration system (schematic map of the whole process shown in **Fig.1**.) and characterizes them with a series of spectroscopic, microscopic and mechanical methods. A simulation model based on Darcy's law has also been discussed to explain why a translucent ceramic can be obtained by this simple system.

2 **Materials and methods**

The synthesis of HA and SrHA nanoparticles can be simplified and described in the reaction scheme shown (Eqn. 1), which is one of the most standard routes of precipitating HA based on the reaction between calcium nitrate and ammonium dihydrogen phosphate[27].

$$5Ca(NO_3)_2 + 3(NH_4)_2HPO_4 \xrightarrow{4NH_4OH} Ca_5(PO4)_3(OH) + 3H_2O + 10NH_4NO_3 \qquad (1)$$

After the nanoparticles are synthesized, a simple filtration system was introduced to achieve translucent HA and SrHA precursors before calcination. Moreover, to better understand the factors contributed to the transparency of such design, the nanoparticle morphologies of different HA precursors, as well as the pressure drop in the precursor layer induced by the total number of accumulated particles, were demonstrated in terms.

2.1 Synthesis and filtration of translucent HA and SrHA

Calcium nitrate, strontium nitrate, diammonium hydrogen phosphate and ammonia solution were purchased from Sigma-Aldrich (USA). All chemicals were analytical grade reagents used as received without further purification.

The vacuum pump systems (D-79112) connected with a filter unit was purchased from KNF Neuberger GmbH, Freiburg, Germany and the polycarbonate filter paper (Whatman® Nuclepore™ Track-Etched Membranes) with a diameter of 47 mm and pore size 0.4 μm was used throughout the whole procedure.

HA nanoparticles were synthesized by a typical precipitation procedure. Diammonium hydrogen phosphate was individually prepared in mixed in deionized water to form a clear solution with a constant concentration of 0.2 M. Calcium nitrate was prepared in deionized water with a constant stoichiometric Ca/P molar ratio of 1.67 for the formation of $Ca_5(PO_4)_3OH$. The molecular formula usually can be written as $Ca_{10}(PO_4)_6(OH)_2$ to denote that the crystal unit cell comprises two entities. The initial pH of each solution was adjusted to 10. Similar to the synthesis of HA nanoparticles, the strontium substituted HA precursor was prepared by the following procedure. Diammonium hydrogen phosphate was prepared with a concentration of 0.2 M. For the formation of 0.05% strontium substituted calcium hydroxyapatite, ($Ca_{9.95}Sr_{0.05}(PO4)_6(OH)_2$) written as 005SrHA in the following), the calculated concentration of calcium nitrate and strontium nitrate is 0.317 M and 0.013 M and both chemicals were mixed in deionized water under stirring. In order to avoid the rapid growth of crystalline grains, the solutions of pure calcium nitrate and mixed calcium nitrate containing strontium nitrate were added to diammonium hydrogen phosphate solution drop-wise. The whole procedure was performed under vigorous stirring overnight. The precipitate was then kept stationary in the mother liquor for another 24 h. In order to explore the consequences on translucency properties attributed to particle size and morphologies, SrHA nanoparticles (25% and 50% calcium has been substituted

by strontium, from here on referred to as 025SrHA and 050SrHA, respectively) were also prepared by utilizing the similar methods.

For the final and also key step of forming the HA and SrHA translucent ceramic precursors, a 20 mL suspension was taken out from each mother liquor and ultrasonicated to insure a homogeneous suspension. The filtrated precipitate was made into a precursor through a simple glassware based filtration system induced by one laboratory pump (P_{max}= 2.4 bar). The samples were dried in air at room temperature after filtration.

2.2 Sintering of as-prepared HA and SrHA translucent ceramics

Four types of HA and calcium replaced strontium doped HA precursors (HA, 005SrHA, 025SrHA, 050SrHA) were dried totally and then taken into an ordinary non-vacuum furnace (Nabertherm GmbH, Germany) for sintering. The samples for sintering were heated at a rate of 5°C/min up to 1000°C and kept at 1000°C for 2 hours in air. Then, the samples were cooled at the same rate to room temperature.

3 Characterizations

For the optical and mechanical measurements, a flat surface is essential and thus a series of grinding and polishing steps were performed. Firstly, the calcined nanoceramic samples were placed and stabilized in epoxy resin while the generated bubbles were driven out by continuous sonication. Then, the solidified samples were carefully polished by using coarse, medium, fine and superfine discs. The samples were rinsed under running tap water during each step and finally cleaned ultrasonically in distilled water to remove surface debris.

3.1 SEM

Scanning Electron Microscopy (FESEM, LEO 1550) was employed to detect the morphologies from four types of HA and SrHA nanoparticles as well as their calcined ceramic structure. To significantly expose the crystalline grain, the polished surfaces from the samples were etched by 15% phosphoric acid for about 15 seconds. The specimens were sputtered with gold before the images were taken.

3.2 TEM

As-prepared calcined disks were sputter coated with a thin layer of Au, and prepared for TEM using a focused ion beam (FIB) microscope with an in situ lift-out method. This method enabled the removal and thinning of an electron transparent lamella, of approximate size 10µm x 4µm x 100nm, from the bulk. Transmission electron microscopy (TEM) and selected area electron diffraction (SAED) were performed on a Titan 80-300kV microscope (FEI Company, The Netherlands) operated at 300kV.

3.3 XRD

The phase characterization of the ceramics before and after calcination was investigated by X-ray diffraction (XRD) using a D5000 (Siemens, Cu Kα1 radiation (λ=1.5418Å)). Diffraction angles (2θ) 5-60° were analyzed using 0.02° as the step size and 2s per step as the scan speed. Rietveld refinement was used to calculate the crystal size of each phase.

3.4 FTIR and UV spectroscopy

FTIR analysis was employed to chemically detect and evaluate the functional groups within precursors and nanoceramic HA, as well as 005SrHA. All FTIR measurements were recorded on a FTIR spectrometer (Bruker IFS 66v/S) equipped with a commercial 1 reflection ATR crystal (SensIR Inc.). Each was typically averaged of 64 scans with a resolution of 4 cm^{-1}. In each experiment the plate sample was pressed by the indenter on top of the ATR crystal. The spectra were baseline corrected and OPUS IR-software (Bruker Optics GmbH) was used for data processing and analysis. The optical transmittance within visible spectrum range was measured on a UV–VIS spectrometer (UV-2501PC, SHIMADZU, Kyoto, Japan).

3.5 Nanoindentation

The hardness and Young's modulus for HA and SrHA translucent ceramics were determined by nanoindentation using an Ultra Nano Hardness tester from CSM instruments with a Berkovich diamond tip. For each specimen, 20 indentations were made using a linear loading profile with a loading rate of 15000μN/min and a max load of 10000 μN. The normally acting force of Fn contact was constantly set as 100 μN. The results are calculated using the method presented by Oliver and Pharr[28]. The standard deviation along with the results was summarized.

4 Pressure filtration model

In order to better understand the attributions to the translucency of the filtrated hydroxyapatite ceramics, a pressure filtration model is summarized and presented here according to Darcy's law. We adapt our simple vacuum pumped filtration system to Darcy's differential equation for fluid flow through porous media[29]. We define the thickness of the consolidated layer as h and constant pressure P generated by the vacuum pump related to the filtration time t. The equation can be described as:

$$t = h^2 \frac{u}{2kP}\left(\frac{v_l - v_0}{v_0}\right)$$

In our case, u is the water viscosity which was used as solvent in the system. v_0 and v_l represent the volume fractions of particulates within the slurry and consolidated precursor layer. k represents the permeability related to the resistance of fluid flow through the consolidated precursor layer. To simplify our filtration system, we assume the HA nanoparticles synthesized from precipitation method are identical nano-spheres with the average diameter of d. Then, based on the Kozeny-Carman relation[30], the permeability can be calculated as:

$$k = \frac{d^2(1-v_l)^3}{36cv_l^2}$$

The Kozeny constant c defines the shape and tortuosity of the flow channels and c= 5 for many systems. Thus, to discuss the relationship between applied pressure P and volume fraction of consolidated precursor layer v_l, we simplify the equation as:

$$p = \frac{h^2 \cdot u}{2t} \cdot \frac{36}{d^2} \cdot \frac{v_l^2}{(1-v_l)^3} \cdot \left(\frac{v_l - v_0}{v_0}\right)$$

To further simplify the equation, we assume

$$A = \frac{h^2 \cdot u}{2t} \cdot \frac{36}{d^2}$$

Then we have

$$p = A \cdot \frac{v_l^2}{(1-v_l)^3} \cdot \left(\frac{v_l - 0.065}{0.065}\right)$$

Here, for the value of v_0, we collect ten samples from slurry suspension and calculated the average value is around 0.065. The average thickness of the filtrated precursor is 0.25 cm and the estimated filtration time for each precursor layer was 90 s. The average diameter of the spheres was approximately 100 nm. Thus, constant value of A=1.11×10^5. Since the HA nanoparticles are randomly distributed in diameter size, we define such sphere assembly behavior as random packing. Finally, we get to the correlation between P and v_l.

Also, from the previous equation we can get the correlation between T and v_l

$$t = B \cdot \frac{v_l^2}{(1-v_l)^3} \cdot \left(\frac{v_l - 0.065}{0.065}\right)$$

Here we assume

$$B = \frac{h^2 \cdot u}{2P} \cdot \frac{36}{d^2}$$

And in our study, we simplify the applied trans-membrane pressure ΔP is the sum of the pressure generated by the pump and external atmosphere P_0. Then $\Delta P = P_{max} + P_0 = 3.4$ bar. Constant B=43.39. Finally, we get the correlation between t and v_l.

5 Results

5.1 Optical images and SEM

The optical images of HA and 005SrHA before and after sintering are shown in **Fig.2**. It can be observed that translucency was obtained after filtration in both plates but decreased after sintering. However, for 025SrHA and 050SrHA precursors, translucency can be hardly detected by eyes. **Fig.3.** shows the morphologies from HA and different strontium substituted HA precursor. The synthesized HA and 005SrHA precursors display spherical morphologies. The ceramics revealed a highly compact structure and inter-granular pores were difficult to detect on either HA and 005SrHA ceramics, see **Fig.4 (A-D)**. However, a significant morphology transformation to rod-like particles was found with increasing strontium concentration in the case of 025SrHA and 050SrHA precursors. Moreover, the grain morphology is mainly between quadrangular to hexagonal with a size in the range of 100 to 300 nm and it is revealed that sintered 025SrHA (**Fig.4 E**) and 050SrHA (**Fig.4 F**) ceramics are highly porous from which the grain boundaries cannot be observed even after surface etching.

5.2 TEM

TEM images of the HA ceramic are shown in **Fig.5 A.** confirm the spherical and highly compact grain structure with grain sizes from approximately 200 nm to 1μm. The ceramic is densely packed and pores were not detected. The polycrystalline nature of the ceramic is confirmed by the SAED pattern in **Fig.5 B**.

5.3 XRD

X-ray diffraction patterns of the ceramics before and after calcination were shown in **Fig.6**. All the ceramics were single phase. The diffraction peaks of HA and 005SrHA were broad before calcination and both of the peaks became sharper after calcination at 1000°C. This indicated that the crystallinity and crystal size increased after calcination. The strongest diffraction of HA and 005SrHA nanoparticles came from (211) plane. The crystal sizes of HA and 005SrHA were 15 nm and 13 nm at (001) plane before calcination, see **table 1**. They increased to 137 nm and 132 nm, which are in the size range from SEM, respectively after calcination.

5.4 FTIR and UV spectroscopy

Fig.7. shows the main infrared band positions and their assignments summarized. The spectra indicate all the HA and SrHA are carbonate substituted types. The peaks at 2344 cm^{-1} and 2362 cm^{-1} are attributed to the absorption of atmospheric CO_2 during the precipitatation of HA particles, which is been described previously in the literature[31]. The long synthesis time and overnight aging would increase the possibility for this substitution to occur. The bands at 1029 cm^{-1} and between the range from 565 cm^{-1} to 630 cm^{-1} represent the presence of orthophosphate

ions among the samples. However, compared with precursor samples, the peaks of phosphate groups at 630 cm^{-1}, 961 cm^{-1}, 1095 cm^{-1} become better resolved in calcined nanoceramic samples due to the high temperature during the calcination process[32]. In addition, with calcination, the water absorbed peak[33] as described around 1645 cm^{-1} is not clearly visible in our results.

The UV-vis transmission spectrum of HA and 005SrHA calcined body with 1mm in thickness is shown in **Fig.8 (A-B)**. The obtained spectrum indicates that the transmittance of such HA body is approaching 60% before calcination and declines to 40% after calcination over the wavelengths of 400-700 nm, whereas 005SrHA is approximately 45% before calcination and 30% after calcination. For all the samples including HA and 005SrHA within the measured wavelength range, the optical transmittance increases from 390 nm to 700 nm, which attributes to the change of the scattering intensity[34].

5.5 Nano indentation

The mechanical properties of the well-polished samples were studied by nano indentation tests, see **Fig.9**. The HA ceramic has the hardness of 9.2 ± 0.3 GPa and the elastic modulus of 145 ± 1.929 GPa, whereas the 005SrHA ceramic has a HIT value of 9.0 ± 0.1 GPa and EIT value of 155 ± 1.641 GPa. The results showed that the pure HA ceramic has a slightly higher hardness than strontium substituted HA.

5.6 Theoretical model

The density of the consolidated precursor will finally determine the density and transmittance of the HA ceramic. It is important to know how to get the precursor as dense as possible by simply altering filtration time and pressure. **Fig.10A.** showed the correlation between volume fractions of particulates within the consolidated precursor layer v_l and filtration time T. In the beginning of filtration, there is a shape growth for the particulates within the consolidated layer. However, such growth is gradually reduced after a period of time. The same tendency is also found in **Fig.10B**, which showed the correlation between volume fractions of particulates within the consolidated precursor layer v_l and trans-membrane pressure ΔP.

6 Discussions

The low refractive index and extremely small birefringence[35] ($n\omega = 1.651$, $n\varepsilon = 1.644$, $\delta = 0.007$) of HA make it possible to be fabricated into transparent ceramics. In this work, translucent HA ceramics with considerable optical performance were achieved by a simple vacuum pumped filtration system. One of the novel aspects of this study is that the whole procedure, including the HA precursor synthesis and the final fabrication of translucent HA ceramics, did not require extreme temperature and pressure-assisted conditions, as compared to traditional methods of making such HA ceramics.

This study also indicates the applications of fabricating transparent or translucent materials by controlling the particle morphology. From achieved dried precursors after filtration, the translucency can be seen by eye for both HA and 005SrHA filtrated precursors (**Fig.2.A, C**). However, the translucency cannot be observed in either 025SrHA and 050SrHA dried precursors (**Fig.2.E, F**), which contain rod-shaped particles. The images indicate that nano-sphere agglomeration is more likely to adopt a highly compact structure, which will directly affect the translucency of the ceramic phases. The poor stacking of nano-rod shape particles would thus decrease the translucency of such ceramics due to the increasing amount of porosity. Interestingly, from our current setup the translucent HA and 005SrHA ceramics can also be achieved by applying filter paper with a pore size of 0.2 μm.

Table 2 summarizes previously established methods of fabricating transparent HA ceramics and their reported micro-hardness values[36-38]. The hardness we achieved in our HA ceramic samples showed no lower than 10% increase compared to previous work, demonstrating that the facile filtration method cannot just maintain, but indeed slightly improve the mechanical properties of HA ceramics which presents many advantages for applications.

The pores, grain size and grain boundaries of a ceramic are the main factors to affect its translucency and mechanical strength. The porosity is the most important factor for the translucency of the material, and porosity lower than 0.1% can obtain an initial transparency[34]. To explore our practical system in affecting the translucent precursor layer, a model combing pressure drop and precursor formation process has been introduced here. For spherical close random packing, the ideal packing density should be in the range of 0.625 to 0.641[39]. In our model as shown in **Fig.10**, to achieve a theoretical ideal close random packing, the trans-membrane pressure ΔP has to reach as almost high as 5×10^6 Pa and 25 minutes filtration. In this experiment, the highest pressure we can get is 3.4×10^5 Pa, and there will be cracks if the filtration time is longer than 3 minutes, and if cracks form, the high pressure will be lost. Therefore, with our current setup, the maximum packing density that can be reached is only approximately 0.4. Therefore, it becomes interesting to understand why the translucent ceramics can still be obtained from the above process at a below ideal packing density. The precursors of HA and 005SrHA showing a certain transparency are mainly due to the water existing between spherical nanoparticles in the green bodies, which could induce less diffraction at the interface of ceramic and water than the diffraction at the interface of ceramics and air. During the drying process, capillary forces help to densify the precursors and the packing density will be increased. In this study, the conventional sintering process has been chosen without using vacuum and high pressure. The elimination of pores mainly depends on the crystal growth which can push pores existing between crystals out. Because the green body was composed of spherical nanoparticles, the mass transformation and growth of grain boundaries is more homogeneous than green bodies with rods and irregular shaped grains. Sintering under vacuum may help to achieve a higher translucency. Based on the results in this study, by controlling the morphology of ceramic nanoparticles, other functional translucent ceramics could be fabricated via this simple technique.

7 Conclusions

Two types of translucent ceramics, HA and 0.05% strontium substituted calcium HA, were successfully fabricated by a simple filtration method. Optical transmittance tests confirmed that the translucency of each body was mostly retained after calcination at 1000°C, and both ceramics achieved commercialized mechanical properties. By contrast, 25% and 50% Sr substituted HA nanoparticles and ceramics were also synthesized but the filtered bodies as well as the calcined ceramics were opaque. We contribute such difference to the change of nanoparticle morphology from spherical to rod-like with increasing Sr concentration and the decreasing packing density of the filtrated precursor associated with this change. The morphology of nanoparticles is one of the key factors to prepare translucent ceramics via such a simple method. The theoretical model presented confirms the importance of a proper filtration pressure and time to produce a dense precursor and finally a sintered translucent ceramics.

Acknowledgements

This project is supported by Carl Tryggers Stiftelse (CTS 14:525). We gratefully acknowledge China Scholarship Council (CSC) for PhD fellowship. Transmission Electron Microscopy was performed at the Canadian Centre for Electron Microscopy at McMaster University, a facility supported by NSERC and other government agencies.

References

1. G. H. Beall and D. A. Duke, *J. Mater. Sci.*, 1969, **4**, 340–352.

2. a. V. Belyakov and a. N. Sukhozhak, *Glas. Ceram.*, 1995, **52**, 14–19.

3. F. Burny, M. Donkerwolcke, F. Moulart, R. Bourgois, R. Puers, K. Van Schuylenbergh, M. Barbosa, O. Paiva, F. Rodes, J. . Bégueret, and P. Lawes, *Med. Eng. Phys.*, 2000, **22**, 469–479.

4. Doremus R H, *J. Mater. Sci.*, 1992, **27**, 285–297.

5. R. Chaim, R. Marder-Jaeckel, and J. Z. Shen, *Mater. Sci. Eng. A*, 2006, **429**, 74–78.

6. Q. Chen, Y. Shi, L. An, J. Chen, and J. Shi, *J. Am. Ceram. Soc.*, 2006, **89**, 2038–2042.

7. M. Eriksson, Y. Liu, J. Hu, L. Gao, M. Nygren, and Z. Shen, *J. Eur. Ceram. Soc.*, 2011, **31**, 1533–1540.

8. S. V. Dorozhkin and M. Epple, *Angew. Chemie - Int. Ed.*, 2002, 41, 3130–3146.

9. S. V. Dorozhkin, *Materials (Basel).*, 2009, 2, 399–498.

10. M. Bohner, *Injury*, 2000, 31.

11. B. Locardi, U. E. Pazzaglia, C. Gabbi, and B. Profilo, *Biomaterials*, 1993, **14**, 437–441.

12. S. V. Dorozhkin, *J. Mater. Sci. Mater. Med.*, 2013, **24**, 1335–1363.

13. M. Vallet-Regí and J. M. González-Calbet, *Prog. Solid State Chem.*, 2004, 32, 1–31.

14. K. Takikawa and M. Akao, *J. Mater. Sci. Mater. Med.*, 1996, **7**, 439–445.

15. A. John, H. K. Varma, S. Vijayan, A. Bernhardt, A. Lode, A. Vogel, B. Burmeister, T. Hanke, H. Domaschke, and M. Gelinsky, *Biomed. Mater.*, 2009, **4**, 015007.

16. N. Kotobuki, K. Ioku, D. Kawagoe, H. Fujimori, S. Goto, and H. Ohgushi, *Biomaterials*, 2005, **26**, 779–85.

17. D. Kawagoe, Y. Koga, E. H. Ishida, N. Kotobuki, H. Ohgushi, and K. Ioku, *Phosphorus Res. Bull.*, 2006, **20**, 119–128.

18. H. Aoki, M. Akao, Y. Shin, T. Tsuzi, and T. Togawa, *Med. Prog. Technol.*, 1987, **12**, 213–220.

19. A. a Chaudhry, H. Yan, K. Gong, F. Inam, G. Viola, M. J. Reece, J. B. M. Goodall, I. ur Rehman, F. K. McNeil-Watson, J. C. W. Corbett, J. C. Knowles, and J. a Darr, *Acta Biomater.*, 2011, **7**, 791–9.

20. B. N. Kim, E. Prajatelistia, Y. H. Han, H. W. Son, Y. Sakka, and S. Kim, *Scr. Mater.*, 2013, **69**, 366–369.

21. L. Boilet, M. Descamps, E. Rguiti, A. Tricoteaux, J. Lu, F. Petit, V. Lardot, F. Cambier, and A. Leriche, *Ceram. Int.*, 2013, **39**, 283–288.

22. K. Uematsu, M. Takagi, T. Honda, N. Uchida, and K. Saito, *J. Am. Ceram. Soc.*, 1989, **72**, 1476–1478.

23. M. Takagi, M. Mochida, N. Uchida, K. Saito, and K. Uematsu, *J. Mater. Sci. Mater. Med.*, 1992, **3**, 199–203.

24. H. Search, C. Journals, A. Contact, M. Iopscience, and I. P. Address, **107**.

25. Y. Fang, D. K. Agrawal, D. M. Roy, and R. Roy, 1995, **23**, 147–151.

26. Y. Watanabe, T. Ikoma, A. Monkawa, Y. Suetsugu, H. Yamada, J. Tanaka, and Y. Moriyoshi, *J. Am. Ceram. Soc.*, 2004, **88**, 243–245.

27. I. Arita, E. Rivera, and V. M. Castano, *J. Mater.*, 1998, **6**, 2–7.

28. W. C. Oliver and G. M. Pharr, *J. Mater. Res.*, 1992, 7, 1564–1583.

29. F. M. Tiller and C. Tsai, *J. Am. Ceram. Soc.*, 1986, **69**, 882–887.

30. D. B. Marshall and A. G. Evans, *J. Am. Ceram. Soc.*, 1985, **68**, 225–231.

31. S. Nayar, M. K. Sinha, D. Basu, and A. Sinha, *J. Mater. Sci. Mater. Med.*, 2006, **17**, 1063–8.

32. R. N. Panda, M. F. Hsieh, R. J. Chung, and T. S. Chin, *J. Phys. Chem. Solids*, 2003, **64**, 193–199.

33. R. Kumar, K. H. Prakash, P. Cheang, and K. A. Khor, 2004, **8**, 5196–5200.

34. R. Apetz and M. P. B. Bruggen, *J. Am. Ceram. Soc.*, 2003, **86**, 480–486.

35. D. Holzmann, D. Holzinger, G. Hesser, T. Schmidt, and G. Knör, *J. Mater. Chem.*, 2009, **19**, 8102.

36. N. Tan, Z. Kou, Y. Ding, Y. Leng, C. Liu, and D. He, *Scr. Mater*., 2011, **65**, 819–822.

37. H. Varma, S. P. Vijayan, and S. S. Babu, *J. Am. Ceram. Soc*., 2004, **85**, 493–495.

38. N. Velisavljevic and Y. K. Vohra, *Appl. Phys. Lett*., 2003, **82**, 4271–4273.

39. F. Dullien, Porous media: fluid transport and pore structure, 2012.

Figures and Tables

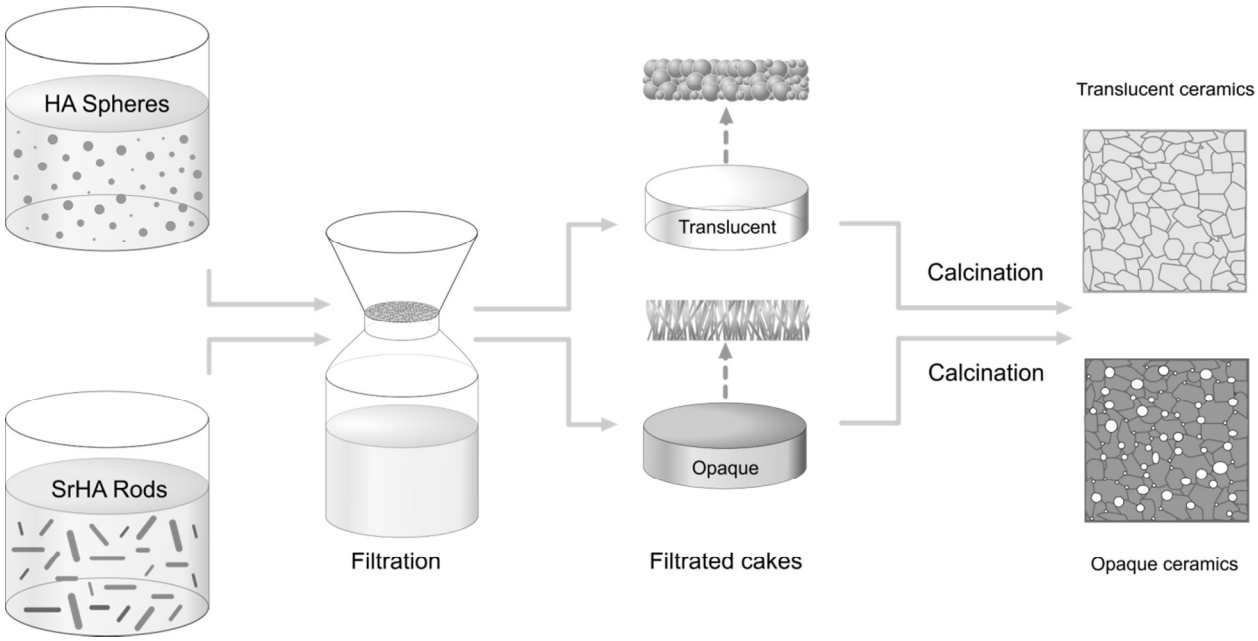

Figure 1 Schematic map of the whole process of preparation of translucent hydroxyapatite ceramics

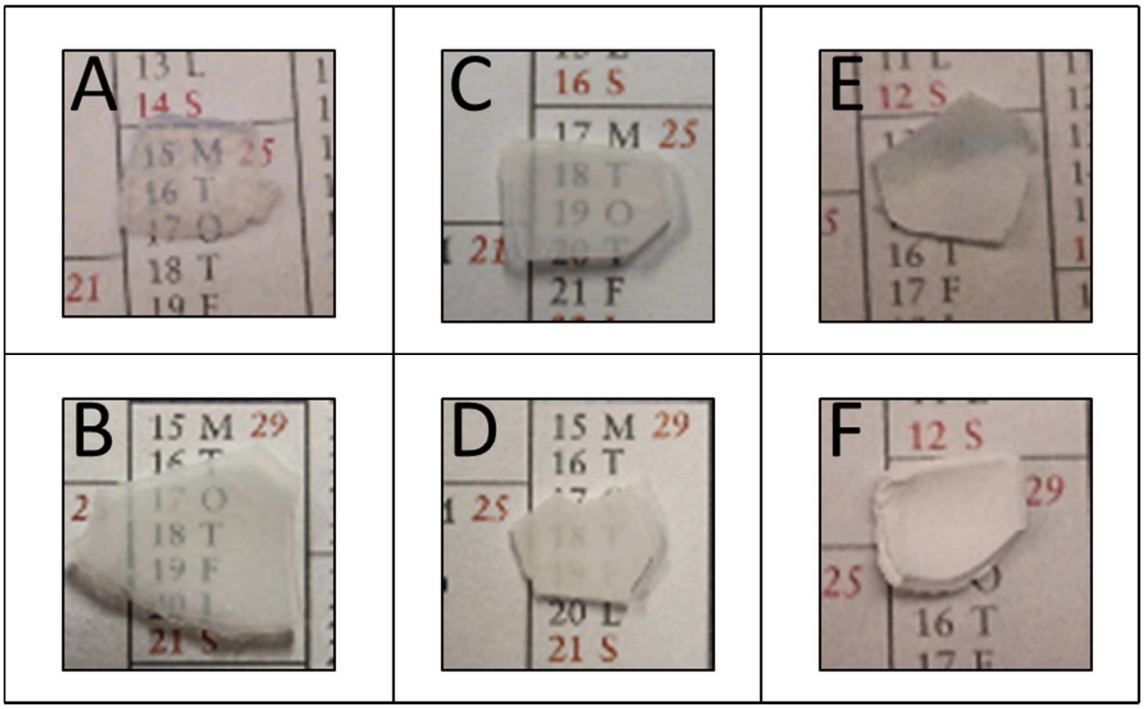

Figure 2 Opitical images of HA precursor cake (A), HA ceramic (B), 005SrHA precursor cake (C), 005SrHA ceramic (D), 025SrHA precursor cake (E), 050SrHA precursor cake (F).

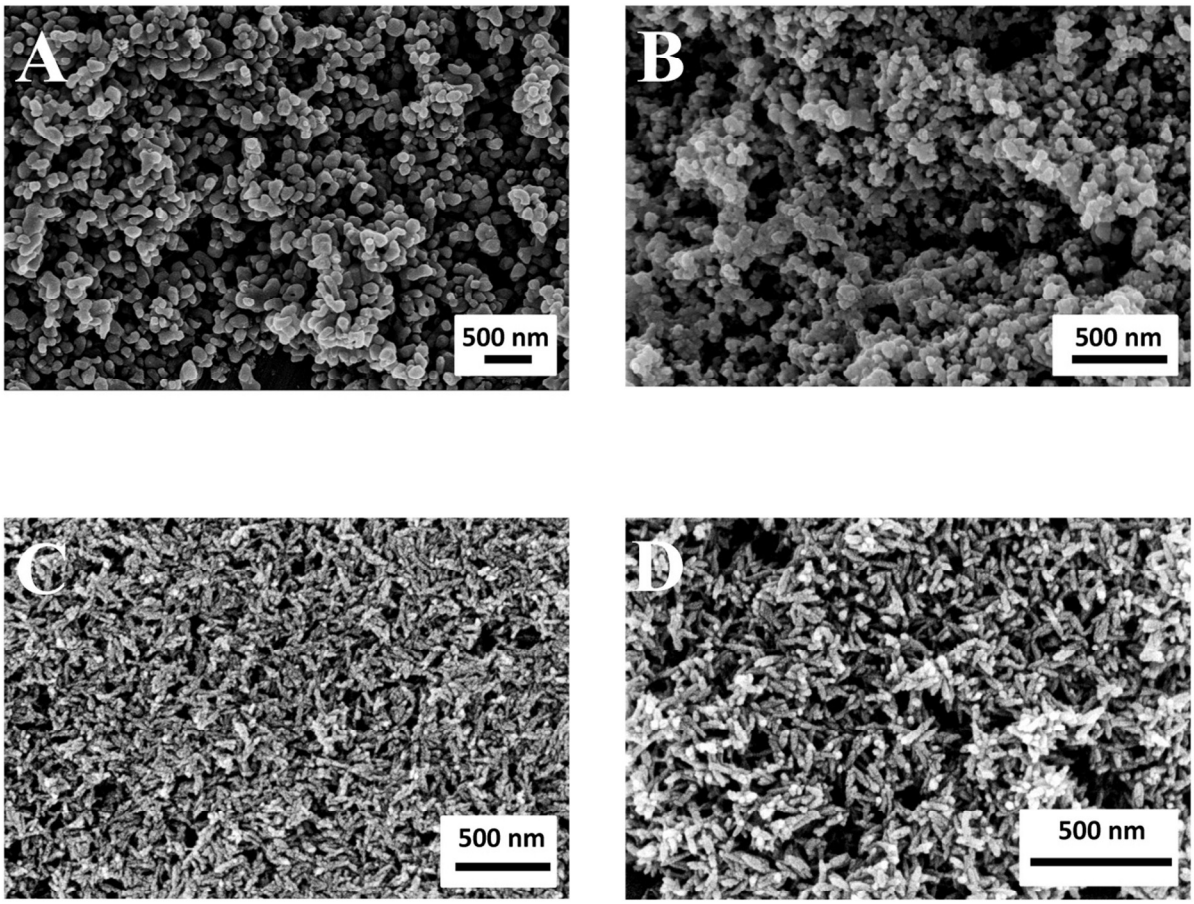

Figure 3 The morphologies of the precursors as revealed by SEM (A) HA (B) 005SrHA, (C) 025SrHA, (D) 050SrHA. With increasing strontium concentration a shift from spherical to rod/like morphology is seen.

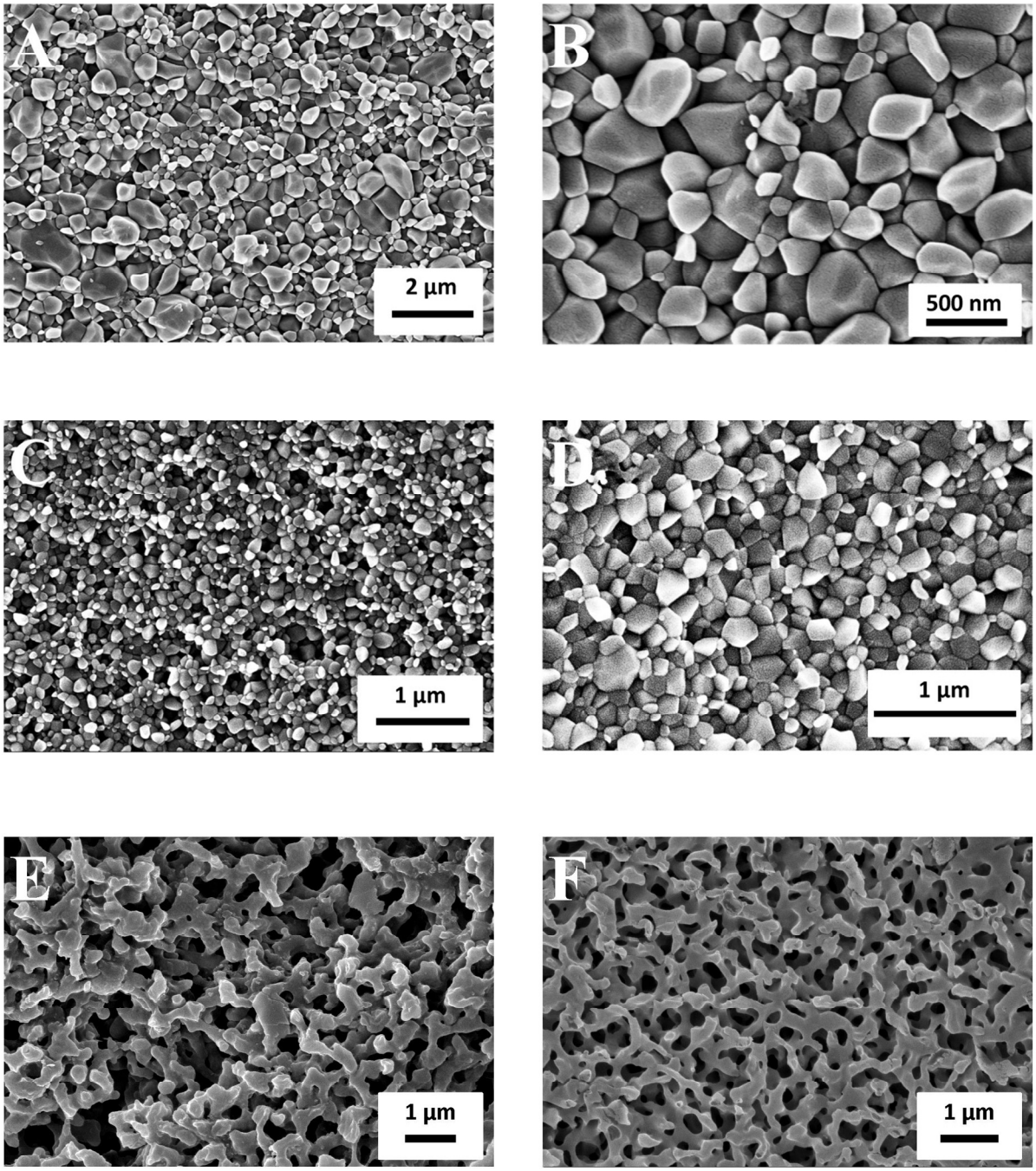

Figure 4 The morphologies of the ceramic specimen as revealed by SEM (A) low magnification HA, (B) High magnification HA, (C) low magnification 005SrHA, (D) high magnification 005SrHA, (E) 025SrHA, (F) 050SrHA

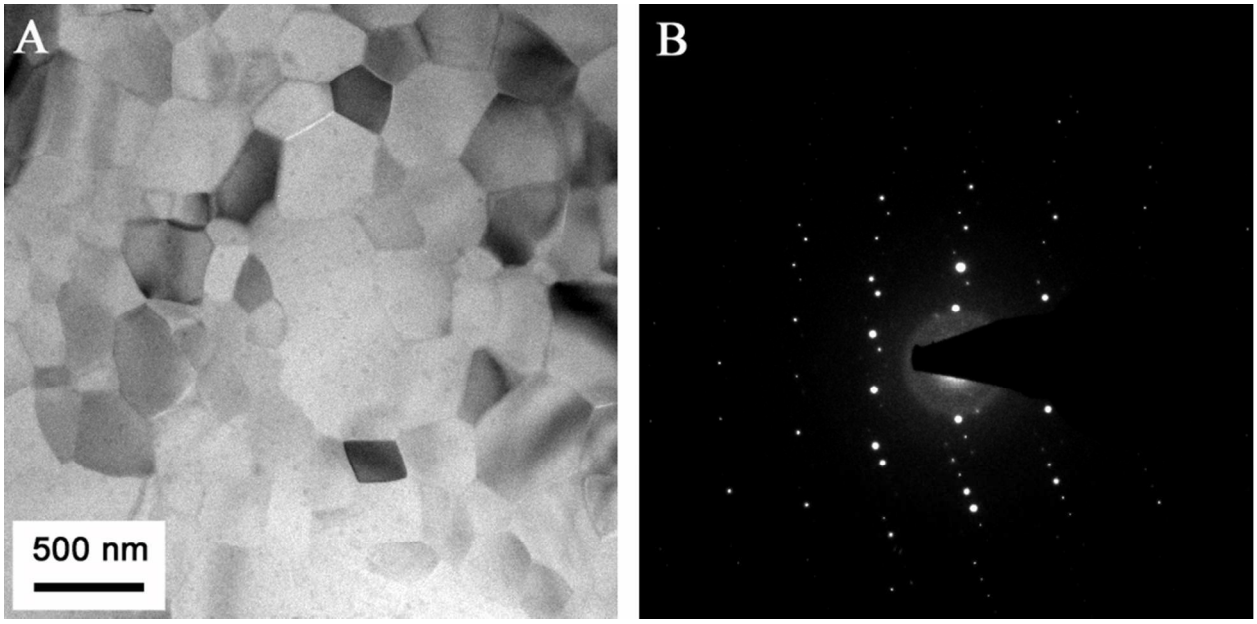

Figure 5 TEM image of the HA ceramic (A), and corresponding selected area electron diffraction pattern (B) showing the polycrystalline nature of the sample with grains ranging from 200nm to 1μm.

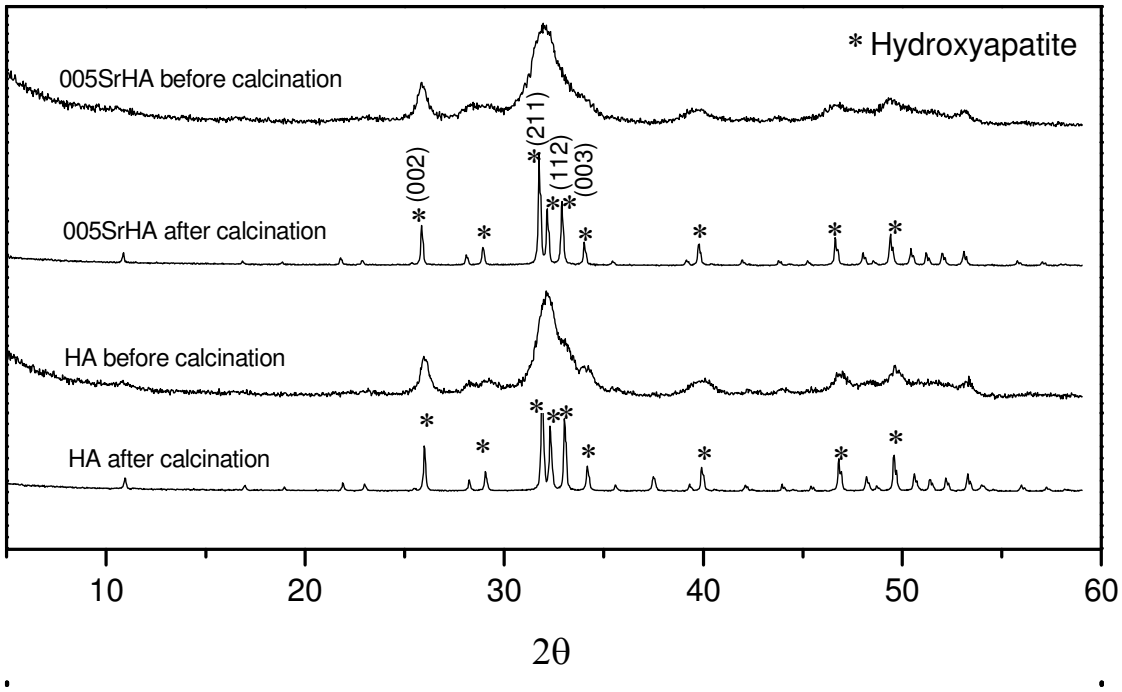

Figure 6 XRD pattern of the ceramics before and after calcination for HA and 005SrHA

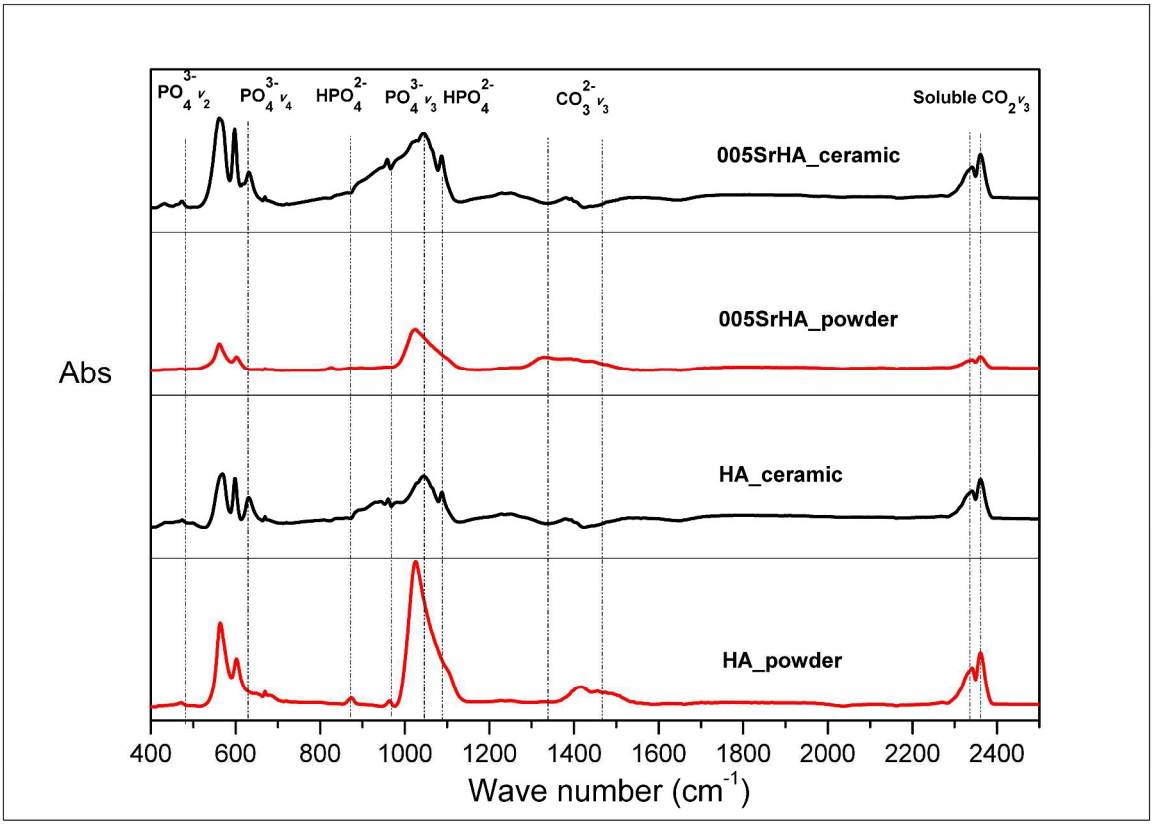

Figure 7 The FTIR spectra of HA and 005SrHA in powder and ceramic specimen.

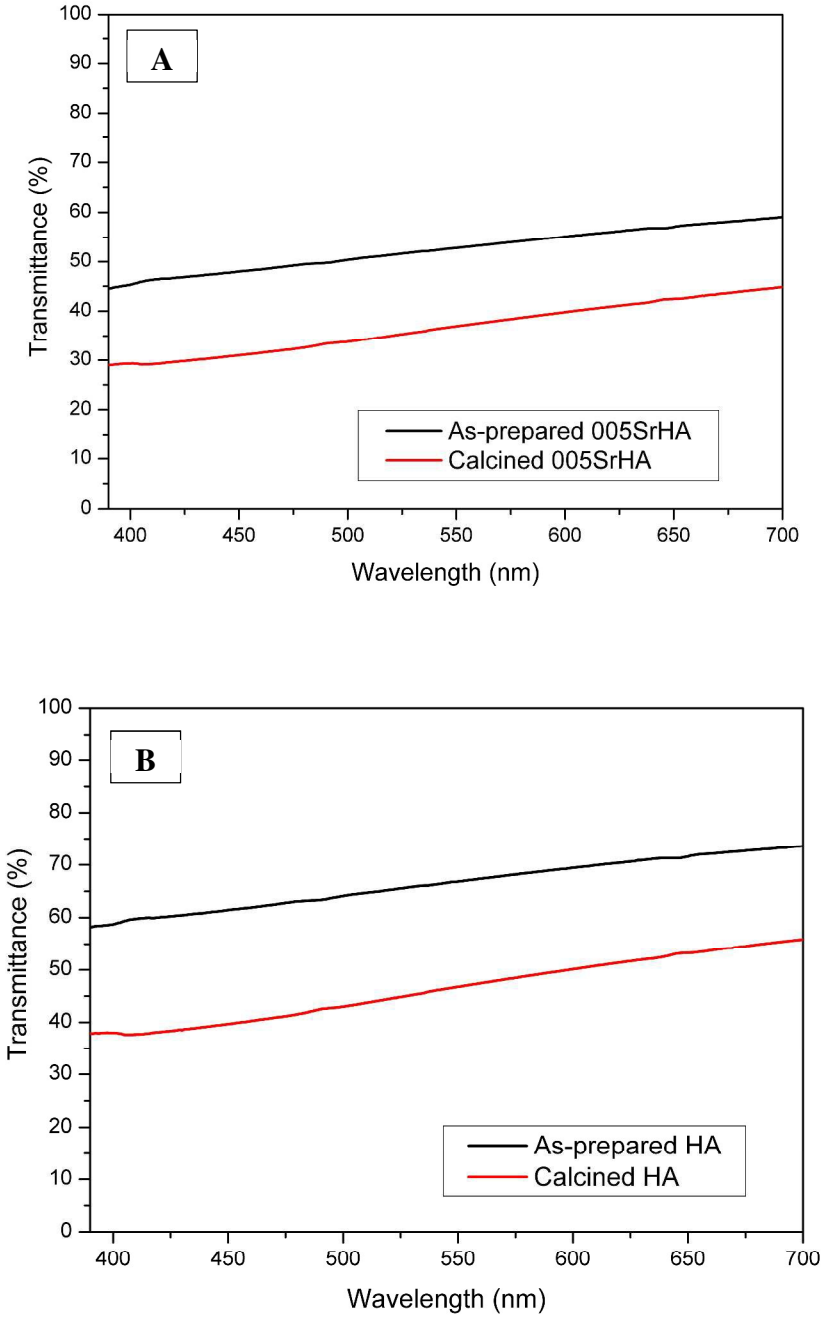

Figure 8 The transmission of the nanocrystalline HA (A) and 005SrHA ceramics (B) as a function of the wavelength of visible light. Calcination decreases the optical transmittance.

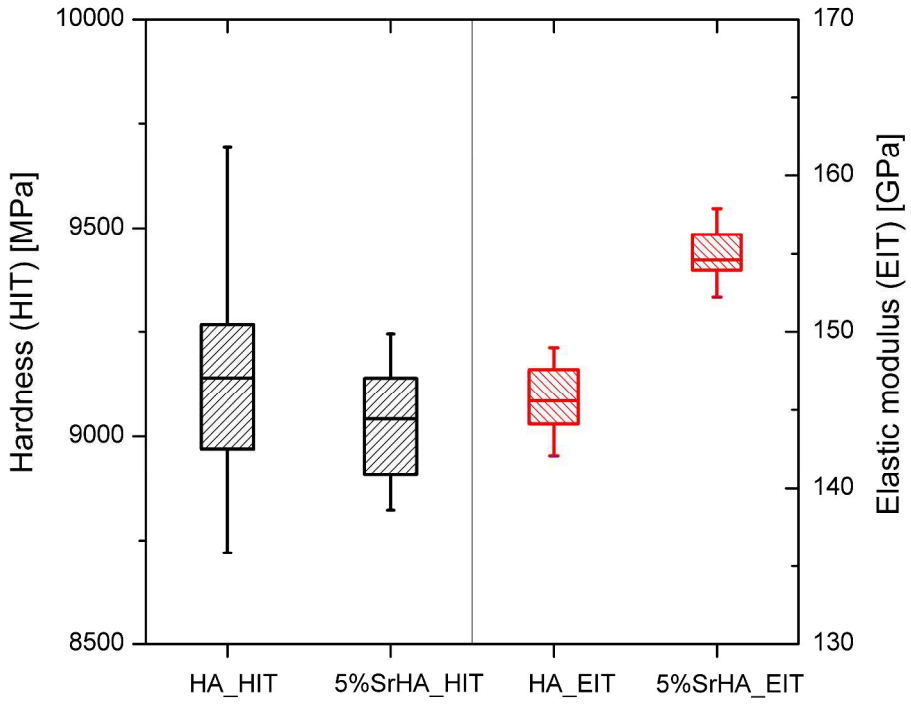

Figure 9 The hardness and elastic modulus of the HA and 005SrHA ceramic specimen as revealed by nanoindentation, 5%SrHA: 005SrHA, 5%SrHA: 050SrHA.

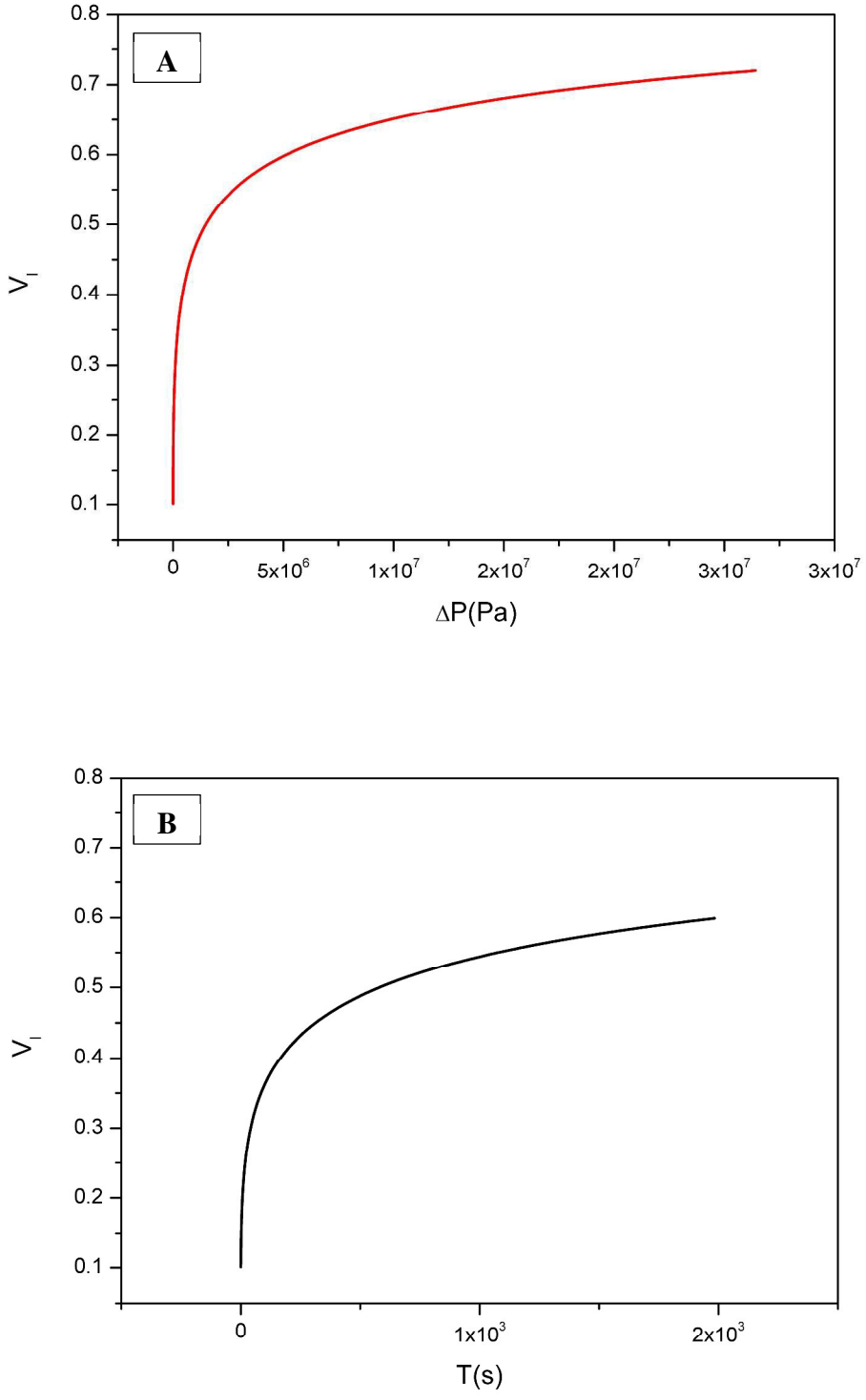

Figure 10 the correlation between P and v_l (A) and the correlation between t and v_l (B)

Table 1 Crystal size of sintered translucent HA ceramics

Crystal size (nm)	(001)	(100)
SrHA(before calcination)	13	6
SrHA(after calcination)	132	117
HA(before calcination)	15	8
HA(after calcination)	137	118

Table 2 Hardness of different translucent HA from literatures and this study

Hardness (GPa)	Fabrication Method	Pressure (GPa)	Temperature (℃)	Refs
9.2 ± 0.3	Simple filtration + Calcination	Ambient	1000	This work
7.9 ± 0.3		3.0	435	
8.0 ± 0.4	UHP sintering	4.0	385	[36]
6.57 ± 0.55	Gelcasting + Sintering	Ambient	1000	[37]
3.5-4.4	Obtained from Plasma Biotal Ltd., UK	11-30	r. t.	[38]

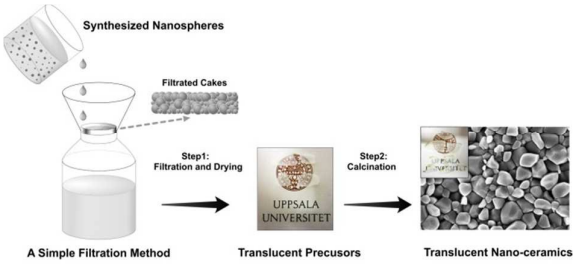

Translucent nano-ceramics fabricated by a simple filtration method followed by a regular sintering process. The key factors are the morphology of nanoparticles and pressure of filtration.